Nanoscale

Accepted Manuscript

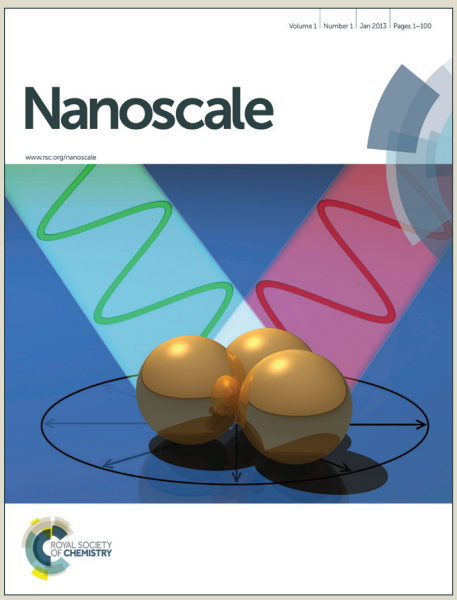

ROYAL SOCIETY OF CHEMISTRY

www.rsc.org/nanoscale

Nanoscale

RSCPublishing

PAPER

Porous carbon nitride nanosheets for enhanced photocatalytic activities†

Cite this: DOI: 10.1039/x0xx00000x

Jindui Hong,[ab] Shengming Yin,[ab] Yunxiang Pan,[a] Jianyu Han,[ab] Tianhua Zhou[ab] and Rong Xu*[ab]

Received 00th September 2014,
Accepted 00th September 2014

DOI: 10.1039/x0xx00000x

www.rsc.org/

Porous carbon nitride nanosheets (PCNs) have been prepared for the first time by a simple liquid exfoliation method *via* probe sonication. These mesoporous nanosheets of around 5 nm in thickness combine several advantages including high surface area, enhanced light absorption and excellent water dispersity. It can be used as a versatile support for co-catalysts loading for photocatalytic dye degradation and water reduction. With 3.8 wt% Co_3O_4 loaded, PCNs can achieve more efficient photocatalytic degradation of Rhodamine B, compared with non-porous C_3N_4 nanosheets (CNs), bulk porous C_3N_4 (PCN) and bulk nonporous C_3N_4 (CN). With 1.0 wt% Pt loaded, CNs and PCN exhibit 7~8 times enhancement in H_2 evolution than CN. Remarkably, PCNs with both porous and nanosheet-like features achieves 26 times higher activity in H_2 evolution than CN. These significant improvements in photocatalytic activities can be attributed to the high surface area as well as better electron mobility of the two-dimensional nanostructure.

1. Introduction

Two-dimensional (2D) materials with a few atomic layers have received increasing interests due to their superior properties for various applications.[1-5] Since the discovery of graphene,[6] other 2D materials, such as nanosheets of MoS_2,[7] WS_2,[8] other transition metal dichalcogenide,[4] covalent framework (COF), etc.,[9] have also been fabricated *via* delamination of their bulk materials. In particular for solar energy conversion and environmental applications, 2D materials have the advantages of higher surface area, improved charge transport ability and more exposed active sites.[4,10-13] For example, monolayered WS_2 nanosheets can be obtained from chemical exfoliation of bulk WS_2 and display more efficient H_2 evolution activity due to more abundant active sites on the nanosheets.[4] In another work, 2D titania nanosheets with a thickness of *ca.* 20 nm were fabricated and hybridized with CdS nanoparticles.[13] These 2D hetero-structures have large surface areas and abundant coupling interface which manifest superior migration of photoexcited charges and excellent H_2 production.[13]

Recently, polymeric-like carbon nitride (C_3N_4) was reported for photocatalytic water reduction and oxidation,[14-18] degradation of pollutants[16,19] and carbon dioxide reduction.[20-23] C_3N_4 nanosheets have been prepared through thermal treatment[10] or liquid exfoliation methods,[24] and studied in diverse applications such as bioimaging,[24] water reduction,[10-12,25], dye degradation[12,24], Cu^{2+} detection[26,27], nanosensor for glucose detection,[28,29] and oxygen reduction reaction.[30,31] Graphene-like C_3N_4 nanosheets were obtained from thermal oxidation of bulk C_3N_4 with improved photocatalytic activities of •OH radical generation and H_2 evolution.[10] From pyrolysis of urea as reported in our previous work, 2D C_3N_4 nanosheets with a high surface area can be obtained and used for improved dye-sensitized H_2 evolution.[25] Besides the thermal process, liquid exfoliation is another facile method to prepare C_3N_4 nanosheets. Bulk C_3N_4 samples obtained directly from the calcination of precursors like melamine, dicyanamide etc. were treated by ultrasonication to obtain exfoliated C_3N_4 nanosheets.[11,24] The reported yield of C_3N_4 nanosheets from the liquid exfoliation method is typically lower than 15%[27,32] and the resultant C_3N_4 nanosheets are non-porous. On the other hand, porous (microporous, mesoporous or macroporous) C_3N_4 materials have shown improved performances for water reduction or dye degradation due to enhanced light absorption and more efficient charge transfer.[15,17,33-35] For example in our earlier studies, mesoporous C_3N_4 with *in situ* sulfur doping was synthesized from pyrolysis of thiourea by using SiO_2 as the template and showed a high quantum efficiency of 5.8% (at 440 nm) for H_2 evolution.[17] Mesoporous C_3N_4 after loading of NiS was also found active for H_2 evolution without the use of noble metal co-catalysts.[34] Three-dimensional macroporous C_3N_4 was fabricated by Jun *et al.* through calcination of melamine-cyanuric acid or melamine-trithiocyanuric acid complex, which showed enhanced activity for H_2 evolution.[35] To the best of our knowledge, no studies have been reported about exfoliation of porous C_3N_4. It is anticipated that the combination of porous

[a] *School of Chemical & Biomedical Engineering, Nanyang Technological University, 62 Nanyang Drive, Singapore 637459. Fax: 65-67947553; Tel: 65-67906713; E-mail: rxu@ntu.edu.sg*

[b] *SinBeRISE CREATE, National Research Foundation, CREATE Tower level 11, 1 Create Way, Singapore 138602*

†*Electronic supplementary information (ESI) available: SEM, TEM and AFM images, BET isotherms and BJH pore size distribution of samples; Effect of Co_3O_4 loading percentage on the RhB degradation; Exfoliation studies of macroporous carbon nitride; Table of literature studies on dye degradation by C_3N_4; Comparison of probe sonication with bath sonication. See DOI: 10.1039/b000000x/*

and nanosheet-like structure in C_3N_4 can lead to both higher surface area for co-catalyst loading, dye molecule adsorption and improved electron mobility. Hence, more efficient photocatalytic activities can be expected.

Herein, we report the preparation of porous C_3N_4 nanosheets *via* a simple liquid exfoliation method by probe sonication. The obtained porous C_3N_4 nanosheets were further loaded with transition metal oxides for photocatalytic degradation of Rhodamine B (RhB) and Pt for water reduction.

2. Experimental

2.1. Preparation of porous carbon nitride nanosheets

Mesoporous C_3N_4 (PCN) and non-porous C_3N_4 (CN) were prepared using similar methods in our previous report.[17] Briefly, cyanamide was calcined at 550 °C for 4 h to obtain CN. The crucible with a lid covered was used to maintain the calcination process in static air. To prepare PCN, cyanamide mixed with SiO_2 (Ludox® HS40, Aldrich, diameter: 12 nm, 40 wt%, mass ratio of cyanamide: SiO_2 = 1: 1) was firstly calcined under the same condition. SiO_2 was removed by etching with hydrofluoric acid solution (HF, 5 wt%, 40 mL, Alfa Aesar; **CAUTION: HF is highly toxic and should be used with extreme care!**) for 24 h followed by centrifugation and washing for several times. Non-porous C_3N_4 nanosheets (CNs) and mesoporous C_3N_4 nanosheets (PCNs) were obtained by dispersing 50 mg of CN or PCN in 50 mL of ethanol, followed by ultrasonication for 2 h using a 750 W Sonics Vibra-cell at 90% amplitude (model VCX 750, Sonics & Materials, Inc., USA). Other solvents including water, methanol, 1-isopropanol, dimethylformamide, acetone, acetonitrile and 1,4-dioxane were also tested to disperse CN before ultrasonication. It was found that the effect of solvent for dispersion is in the order of: ethanol > methanol, water > isopropanol >> others. Therefore, ethanol was used in all studies in this work. The obtained suspension was centrifuged at 6,000 rpm for 5 min to remove un-exfoliated C_3N_4. The top suspension was separated from the precipitated solids and then centrifuged at 20,000 rpm for 5 min. The collected solid was dried at 60 °C in a vacuum oven for characterization and loading of metal oxide co-catalysts. The suspension obtained after centrifugation at 6,000 rpm was used directly for Pt loading for H_2 evolution. The yield of carbon nitride nanosheets was calculated by dividing the weight of the obtained nanosheets by the initial weight of carbon nitride.

2.2. Loading of metal oxides as co-catalyst

Different transition metal oxides including Co_3O_4, Fe_3O_4, NiO and CuO were investigated as co-catalysts for degradation of organic dye. Co_3O_4 and Fe_3O_4 were firstly prepared according to the previous reports.[36,37] To prepare Co_3O_4, colbalt(II) acetate tetrahydrate ($Co(Ac)_2{\cdot}4H_2O$, 0.5 g) was dissolved in a mixture of 2 mL of H_2O and 23 mL of ethanol at 45 °C. Ammonium solution ($NH_3{\cdot}H_2O$, 28-30%, 2.5 mL) was dropwise added into the above solution under vigorous stirring. The temperature was increased to 80 °C and held for 3 h. The obtained dark suspension was washed with acetone to precipitate the solid. The precipitated Co_3O_4 was re-dispersed in 20 mL of methanol. To prepare Fe_3O_4, iron(III) chloride hexahydrate ($FeCl_3{\cdot}6H_2O$, 8.74 mmol) and iron(II) chloride ($FeCl_2{\cdot}xH_2O$, 4.37 mmol) were mixed in 40 mL of H_2O. The solution was heated to 80 °C with N_2 purging and ammonium solution ($NH_3{\cdot}H_2O$, 28-30%, 5 mL) was dropwise added into the above solution under vigorous stirring. After 30 min, the obtained dark solution was washed with deionized H_2O and re-dispersed in 100 mL of deionized H_2O.

To load Co_3O_4 on PCNs, different volumes (0, 46, 93, 185, 278, 370, 556 μL) of Co_3O_4 suspension (2.1 mg Co_3O_4 per mL methanol) was added into 20 mg PCNs dispersed in 1 mL of methanol. After ultrasonication for 10 min followed by drying at 60 °C to remove methanol, the obtained Co_3O_4/PCNs was calcined in air at 350 °C for 2 h to promote the interaction between Co_3O_4 and PCNs. The same loading method was applied to deposit Co_3O_4 on other carbon nitride samples. Fe_3O_4 was loaded on PCNs by the same method. To load NiO and CuO, nickel(II) nitrate or copper(II) nitrate was added into 20 mg PCNs in 1 mL of H_2O, respectively. After ultrasonication for 10 min and drying at 60 °C to remove H_2O, the precursor was calcined at 350 °C for 2 h to form NiO and CuO loaded PCNs.

2.3. Characterizations

The powder X-ray diffraction (XRD) patterns were obtained from a Bruker D2 diffractometer (Cu Kα, λ = 1.5406 Å, 30 kV and 10 mA). Fourier transform infrared (FTIR) spectra were collected on a Digilab FTS 3100 FTIR in the range of 400 - 4000 cm^{-1} by using a standard KBr disk technique. The morphology of samples was observed by field emission scanning electron microscopy (FESEM, JEOL JSM 6701F) and transmission electron microscopy (TEM, JEOL 3010). Atomic force microscopy (AFM) observation was carried out using a MFP3D microscope (Asylum Research) with a silicon cantilever operating in tapping mode. The surface area was determined from the adsorption isotherm of nitrogen at −196 °C on a Quantachrome Autosorb-6B apparatus using the Brunauer−Emmett−Teller (BET) method. The desorption isotherms were used to determine the pore size distribution by using the Barret-Joyner-Halender (BJH) method. The concentration of Co_3O_4 and Fe_3O_4 suspension and the loading percentage of Co_3O_4 in Co_3O_4/PCNs were determined using inductively coupled plasma atomic emission spectroscopy (ICP-AES) on a Perkin Elmer ICP Optima 2000DV. The UV-vis diffusion reflectance spectra (DRS) were collected on a UV-vis spectroscopy (UV2450, Shimadzu) using $BaSO_4$ as reference. Photoluminescence (PL) spectra were collected from FluoroMax-3 spectrofluorometer (Horiba Jobin Yvon) at room temperature with the excitation wavelength of 333 nm and the excitation/emission slit widths both of 5.0 nm. The samples dispersed in water with a concentration of 0.01 mg mL^{-1} were used for analysis.

2.4. Photocatalytic activity evaluation

For degradation of dye, 5 mg of the catalyst was dispersed in 100 mL of Rhodamine B solution (10 mg L^{-1} RhB). After ultrasonication for 10 min, the suspension was stirred in dark for 2 h to reach the adsorption equilibrium prior to photocatalytic reaction. H_2O_2 was added in the suspension (0.01 M) before turning on the light. A 300 W Xe lamp (Newport) without the use of filter was used as the light source. At different time interval, 1 mL of the suspension was withdrawn and centrifuged at 13,000 rpm to remove the catalyst. The supernatant after centrifugation was diluted two times with H $_2$O. The concentration of RhB was determined using a UV-vis spectroscopy (UV2450, Shimadzu). Photocatalytic H_2 reaction was carried out in a closed circulation system using a Pyrex cell (total volume about 300 mL with a top irradiation area of

around 28 cm^2). In each run, a certain volume of the suspensions (for example, 35 mL of 0.134 mg mL^{-1} PCNs in ethanol) was added with 65 mL of triethanolamine (TEOA) aqueous solution (15 vol%, pH = 8.5). $H_2PtCl_6 \cdot xH_2O$ (50 μL, 1 mg mL^{-1} Pt) was added to the above suspension for *in situ* loading of 1 wt% Pt by photoreduction. A 300 W Xe lamp equipped with a 420 nm cutoff filter (Newport) was used as the visible light source. The reaction cell was kept at room temperature with jacketed circulation of cooling water. The amount of evolved H_2 was determined using an online gas chromatography (Agilent 6890N, Argon as carrier gas, 5Å molecular sieve column, TCD detector).

3. Results and discussion

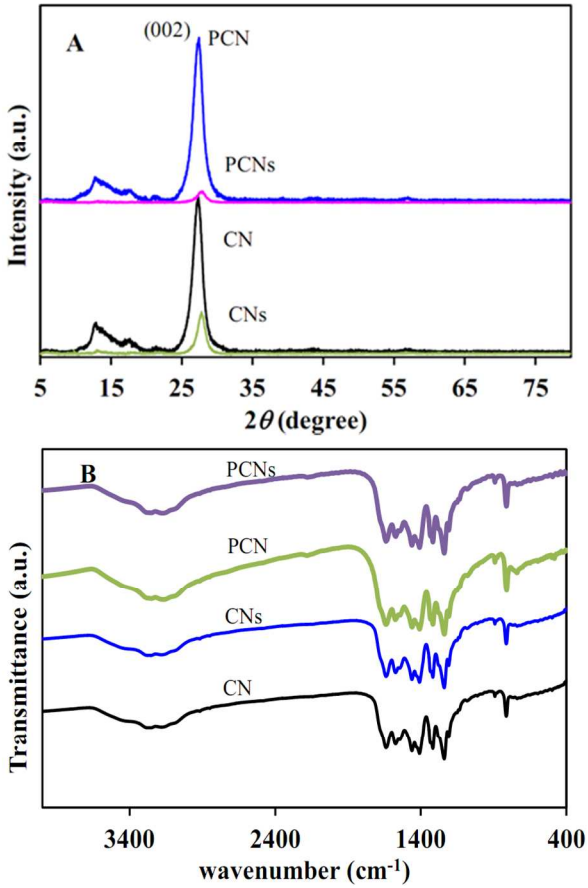

Figure 1. XRD patterns (A) and FTIR spectra (B) of CN, CNs, PCN and PCNs.

Figure 1A shows the XRD patterns of CN, CNs, PCN and PCNs. The intensities of both interlayer-stacking (002) peak and the in-planar peak at 13.3° are greatly reduced after exfoliation of CN and PCN, and the extent of reduction is more severe in the case of PCNs. These results suggest the successful delamination of the bulk CN and PCN.[24] On the other hand, there is no obvious change found in FTIR spectra (Figure 1B), indicating that the functional groups of PCNs and CNs after exfoliation are essentially retained. Both UV-vis DRS and PL spectra reveal a slight blue shift of PCNs and CNs compared with their bulk counterparts, respectively (Figure 2). The blue shift could be due to the quantum confinement effect, which was also shown in previous reports.[10,24] As expected, the porous carbon nitride samples (PCN and PCNs) display

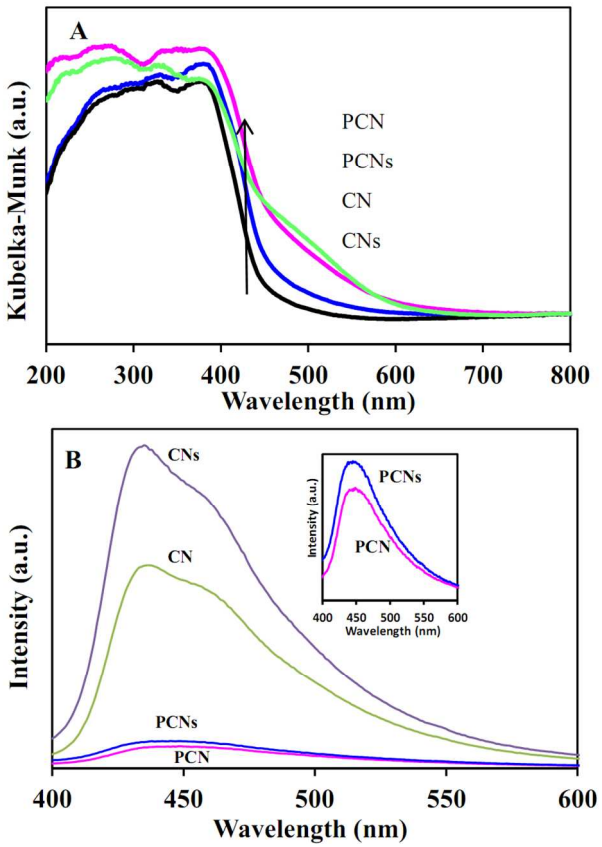

Figure 2. UV-vis DRS spectra (A) and PL spectra (B) of CN, CNs, PCN and PCN and PCNs. PL spectra were recorded under excitation at 333 nm with the inset showing the magnified spectra.

enhanced light absorbance in the visible light range compared to nonporous samples (CN and CNs) due to the scattering sites of pore walls (Figure 2A). Furthermore, it is found that the PL intensities of porous samples are remarkably suppressed compared to those of nonporous carbon nitride samples (Figure 2B). This could be attributed to the presence of more abundant surface defect sites that quench the luminescence.[17] The defect sites were most likely created during the post-treatment by HF acid for removal of SiO_2 template. In our recent study, it was found that the surface defects of metal oxides can enhance the charge separation and promote the photocatalytic activity when the charge carriers can be efficiently utilized by the co-catalysts.[38] Figure 2B also shows that the PL intensities of exfoliated samples are greater than those of the bulk samples, especially for CNs. This may be contributed by a better dispersion of the exfoliated samples in water during PL measurement.

The SEM image in Figure 3A shows that the particle sizes of PCNs are smaller compared to those of the original PCN (Figure S1). The TEM image in Figure 3B indicates that PCNs retains the sheet-like and mesoporous structure despite the reduction in particle size. As shown in Figure 3C, the average thickness of PCNs is around 5 nm, which corresponds to about 14 C-N layers. It is to be noted that this thickness could be overestimated for irregularly shaped particles like PCNs without a large aspect ratio and flat lying surface. A similar morphological change can be found for CNs. The size of the obtained CNs after ultrasonication is decreased roughly to 100-200 nm (Figure S2B and Figure S2D) from the aggregates of

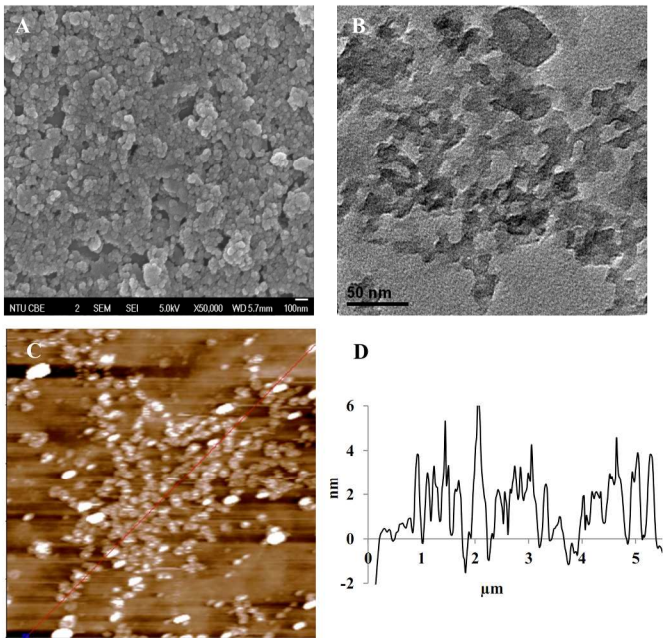

Figure 3. SEM (A), TEM (B), AFM (C) images and height profile of PCNs.

several micrometers of CN (Figure S2A). AFM images in Figure S2C and S2D show that the typical thickness of CNs is around 2-3 nm, corresponding to 5-8 C-N layers. This is similar to those reported in the literature (1.65-2.62 nm,[10] 2 nm,[11] 2.5 nm[24]). Though the same exfoliation conditions were applied to CN and PCN, the thickness of PCNs is roughly twice of that of CNs. Based on TEM observation (Figure 3B), the domain size (i.e., the wall thickness) of PCNs is limited to around 20 nm. It may be challenging for such a small lateral size to induce sufficient interaction between the sample and the solvent for effective exfoliation. On the other hand, the obtained yield of PCNs is 25.8% which is much higher than that of CNs in this work (3.5%) and those in the literature (up to 14.5%).[27,32] This can be well explained by the effect of overall particle size reduction of PCNs which makes the particles better dispersed after ultrasonic treatment. As expected, the samples exhibit larger surface areas after exfoliation. The specific surface area of PNCs is 112.5 m^2 g^{-1} which is 35% higher than that of PCN at 83.4 m^2 g^{-1}. On the other hand, the specific surface area of CNs is increased 2.4 times to 63.9 m^2 g^{-1} compared to that of CN at 18.9 m^2 g^{-1}. These results are consistent with the observed morphological changes. In addition, it is interesting to note that the peak at around 3.9 nm in BJH pore size distribution is greatly enhanced for PCNs compared to PCN (Figure S3B), indicating new pores of smaller sizes were generated during the exfoliation process by ultrasonication.

Co_3O_4 nanoparticles were loaded on PCNs for photocatalytic dye degradation study. XRD patterns in Figure 4A demonstrate the successful preparation of C_3N_4 and Co_3O_4 (JCPDS 78-1970) composites. With the increasing loading percentage of Co_3O_4 in the range of 0.55-7.68 wt% as determined by ICP, the characteristic (311) and (400) peaks of spinel Co_3O_4 become more obvious. The UV-vis DRS spectra (Figure 4B) show that the light absorption intensity in the visible region is greatly enhanced after loading of Co_3O_4 on PCNs. As evidenced by the TEM and HRTEM images in Figure 5, Co_3O_4 nanoparticles of around 5-10 nm are well distributed on the surface of PCNs and the lattices of the

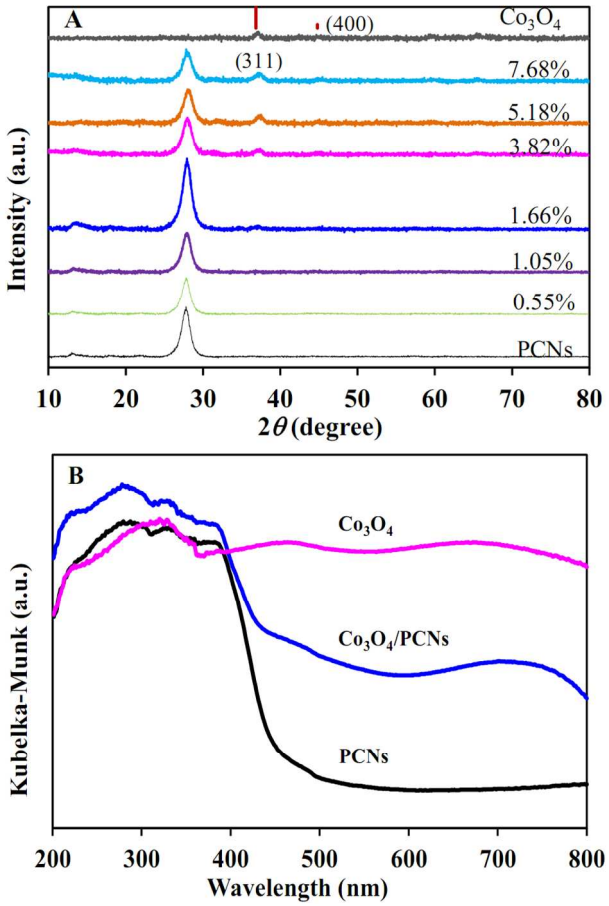

Figure 4. XRD patterns (A) of PCNs, Co_3O_4 and Co_3O_4/PCNs with different weight percentages of Co_3O_4 loaded, and UV-vis DRS spectra (B) of PCNs, Co_3O_4 and 3.82%-Co_3O_4/PCNs. The two lines in (A) indicate the positions of (311) and (400) peak of Co_3O_4 (JCPDS 78-1970).

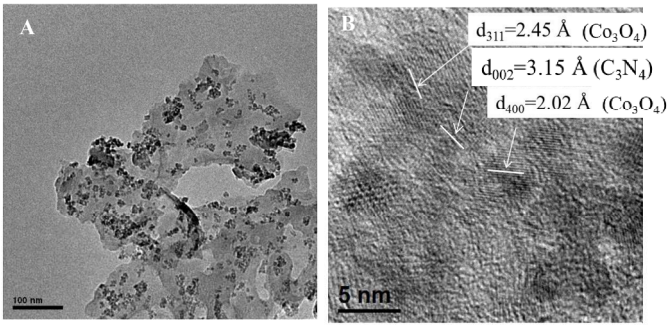

Figure 5. TEM (A) and HRTEM (B) images of 3.82%-Co_3O_4/PCNs.

nanoparticles are consistent with Co_3O_4 phase as detected by XRD. AFM image in Figure S4 shows that particles in 3.82%-Co_3O_4/PCNs become slightly thicker at around 6 nm compared with that of PCNs alone (5 nm) due to the presence of Co_3O_4 on the surface. The mesopores of PCNs could be partially blocked by Co_3O_4 as evidenced by the weakening of BJH peaks in Figure S3B while the specific surface area is only decreased slightly from 112.5 to 103.5 m^2 g^{-1}. Hence, the heat treatment at 350 ^oC during the loading of Co_3O_4 co-catalyst does not induce adverse effects on the morphological properties of PCNs.

Rhodamine B was chosen as a model dye to evaluate the photocatalytic activities of various samples. Before light irradiation, adsorption equilibrium was achieved in the dark. It was found that 2.7%, 4.2%, 8.3% and 10.0% of RhB in the

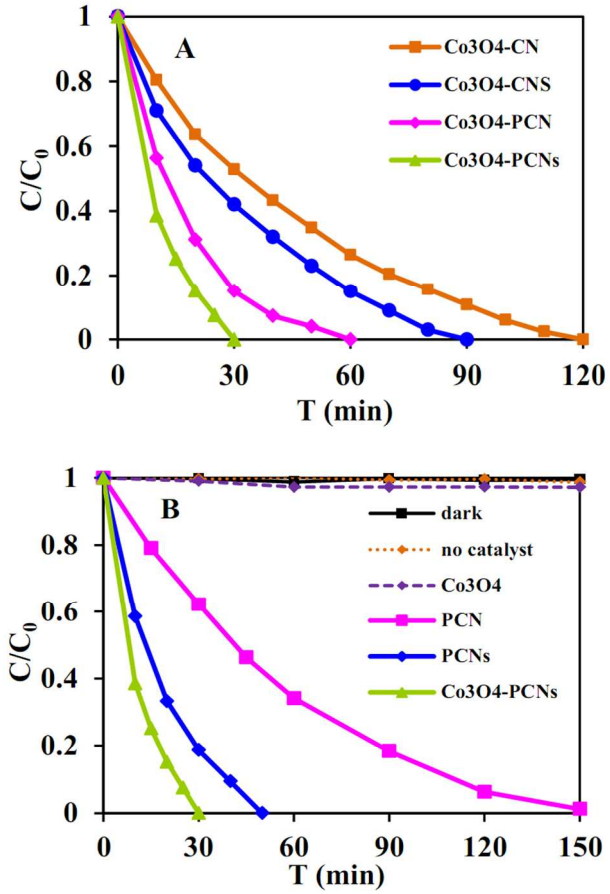

Figure 6. Photocatalytic degradation of RhB over different carbon nitride samples (A) and under different conditions (B) with UV-vis light. The amount of PCN and PCNs were kept at 5 mg, the loading of Co_3O_4 was about 3.8-4.0 wt%.

starting solution can be adsorbed on CN, CNs, PCN and PCNs in the dark, respectively. These results correlate well with the specific surface areas of different samples. Under UV-vis light illumination, RhB can be completely degraded in 2 h when Co_3O_4/CN was used as the photocatalyst and H_2O_2 as the oxidant (Figure 6A). Under the same conditions, it took 30 min less for complete degradation of RhB when CN was replaced by CNs, indicating that exfoliated C_3N_4 with a higher surface area and smaller thickness lead to higher photocatalytic activity, which has been observed by others for degradation of dyes or organic pollutant.[12,24,32] The activity can be further enhanced by using the porous C_3N_4 samples. As shown in Figure 6A, it only requires 60 min and 30 min for complete degradation of RhB in the presence of Co_3O_4/PCN and Co_3O_4/PCNs, respectively. These data show that the photocatalytic activity of C_3N_4 can be greatly improved by proper tuning of its morphological features such as porosity and layer thickness. The mesoporous C_3N_4 nanosheets (PCNs) exhibit remarkably higher photocatalytic activity than the bulk C_3N_4 (CN) due to its higher surface area (Figure S3), enhanced light absorption (Figure 2) and good water dispersity (Figure S5). The control studies (Figure 6B) show that in the absence of light or catalysts, there were no significant changes in dye concentration within 150 min tested. When an equivalent amount of Co_3O_4 alone was used as the catalyst, no appreciable drop in RhB concentration was observed as well. It is to be noted that the catalyst concentration adopted in this work is

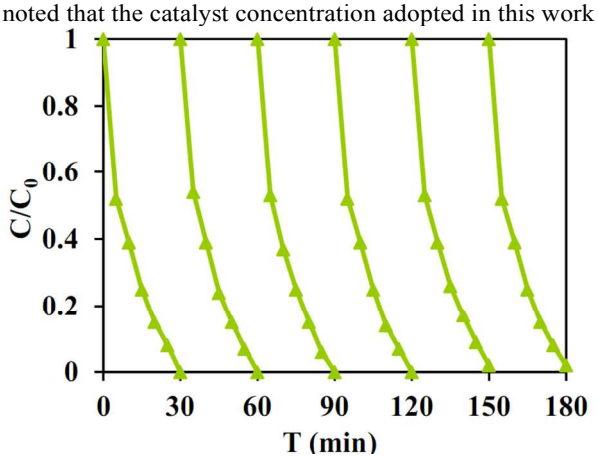

Figure 7. Recycle study of RhB degradation over 3.82%-Co_3O_4/PCNs.

rather low (5 mg of Co_3O_4/PCNs in 100 mL solution). On the other hand, it took 50 min to degrade RhB completely when the bare PCNs was used as the photocatalyst. Thus, the loading of Co_3O_4 can facilitate the electron and hole separation generated in C_3N_4 to achieve higher photocatalytic activity.[4,37] The exfoliated mesoporous C_3N_4 nanosheets developed in the present work can promote the formation of heterostructure with Co_3O_4 due to its high surface area and good dispersity in water. The effect of the loading percentage of Co_3O_4 was studied. As shown in Figure S6, with a small percentage of Co_3O_4 (1.66 wt%) loaded, 61% of RhB can be degraded in 10 min compared with 31% without Co_3O_4. When the loading was increased 3.82%, up to 61% and 85% of RhB can be degraded within 10 and 20 min, respectively. At higher loadings of 5.18% and 7.68%, the activity was dropped which could be due to the light shielding effect caused by the overloaded Co_3O_4 nanoparticles. The time needed for complete RhB degradation was around 30 min when the loading of Co_3O_4 was between 0.55-3.82%. Recycle study using 3.82%-Co_3O_4/PCNs has revealed that the catalyst is stable as there was almost no decrease in activity within 6 cycles (Figure 7). Besides Co_3O_4, three other metal oxides, Fe_3O_4, NiO and CuO, were also loaded on PCNs for degradation of RhB. As revealed by TEM images in Figure S7, these metal oxides were successfully loaded. They have similar particle sizes to that of Co_3O_4 (5-10 nm). Among them, Fe_3O_4 and NiO nanoparticles are poorly dispersed on PCNs compared to Co_3O_4. CuO nanoparticles are well distributed and a similar activity compared with Co_3O_4 for dye degradation was obtained (Figure S8). NiO and Fe_3O_4 as cocatalysts are slightly less active and are still able to degrade RhB completely within 40 min. These results demonstrate that PCNs can be used as a versatile support to load earth-abundant metal oxides for efficient dye degradation. Similarly, macroporous C_3N_4 nanosheets was also prepared by exfoliating macroporous C_3N_4 in the present study. The resultant nanosheets also show enhanced photocatalytic activity for RhB degradation (Figure S9). Although a direct comparison of photocatalytic activity with those in the literature is difficult due to varied reaction conditions, our system is indeed among the best reported under similar reaction conditions as summarized in Table S1.

Based on the results presented in the literature, it was found that bath sonication was generally applied for exfoliation of

C_3N_4. Although this type of sonicator is easily accessible, the relatively weak power and uneven energy distribution within the bath may hamper the efficient production of high quality nanosheets.[13,39] On the other hand, probe sonicator which has a higher power and directly contacts with the liquid can induce higher stress to the liquid in the suspension. Herein, we carried

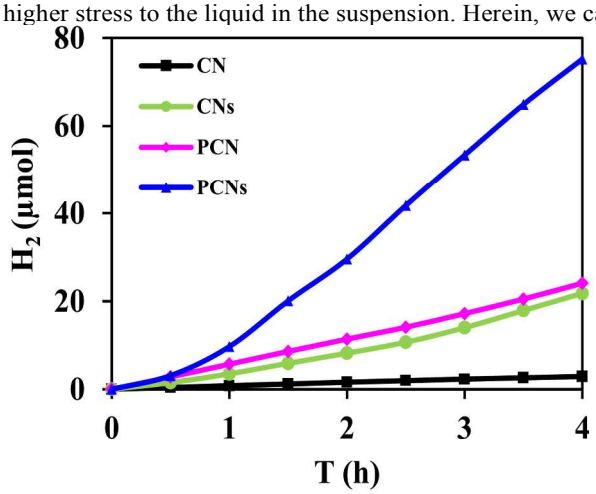

Figure 8. Photocatalytic H_2 evolution under visible light (λ > 420 nm) over Pt/CN, Pt/CNs, Pt/PCN and Pt/PCNs. The amount of catalysts were kept at 5 mg and the Pt loading was 1 wt%.

out a comparative study on these two types of sonicators using PCN sample. The detailed experimental conditions can be found in Supporting Information. Though it is not likely to gain quantitative conclusions for two different systems, it is certain that a much shorter time is needed for probe sonication (2 h) than bath sonication (16 h) to obtain C_3N_4 with similar thickness of several nanometers (Figure S10). Furthermore, probe sonication has resulted in a decrease of lateral size of C_3N_4 to around 200 nm while the bath sonication has no such effect. Micron-sized C_3N_4 nanosheets were mainly observed after bath sonication which is supported by the particle size distribution from dynamic light scattering (DLS) measurement (Figure S10C and D). As a result, the photocatalytic activity of PCNs by probe sonication is higher than that by path sonication for RhB degradation as shown in Figure S10B.

The superior performance of PCNs can also be demonstrated for photocatalytic water reduction to H_2 after loaded with Pt co-catalyst. As shown in Figure 8, the visible light-driven H_2 evolution rate over Pt/PCNs is 18.8 μmol h^{-1}, which is 26 times higher than that over Pt/CN. Meanwhile, Pt/CNs can achieve 7.5 times enhancement in H_2 evolution compared with Pt/CN. The enhancement factor of Pt/CNs compared to Pt/CN for H_2 evolution reported by other groups is normally 2-3 times under visible light.[10,12] Due to the quantum confinement effect, exfoliated C_3N_4 exhibits blue shift in light absorbance with the absorption edge normally shifted from around 450-470 nm to 420 nm.[10,12] Such a blue shift compromises the activity under visible light, hence leading to limited improvement in H_2 evolution as reported in literature. In comparison, the absorbance edges of CNs and PCNs derived from cyanamide in this work after exfoliation are still maintained in the visible light range (456 nm and 488 nm, respectively). As a result, a greater enhancement factor in H_2 evolution activity was obtained in this work under visible light. When urea-derived C_3N_4 was used as a control, a similar blue shift to near-UV light can be observed for exfoliated C_3N_4 which resulted in less than two times enhancement for H_2 evolution (data not shown). These results demonstrate that C_3N_4 obtained from appropriate precursors like cyanamide can benefit more from the formation of nanosheets by exfoliation while with less significant effect from the blue shift due to the 2D quantum confinement.

4. Conclusion

In conclusion, we have demonstrated that the porous C_3N_4 nanosheets (PCNs) obtained by probe ultrasonication treatment of porous C_3N_4 exhibit remarkably enhanced photocatalytic activities compared with the bulk nonporous C_3N_4. With Co_3O_4 loaded as the co-catalyst, the degradation of RhB was completed in 30 min, which is substantially shorter than 120 min required when the bulk C_3N_4 was used. The stability of the catalyst was demonstrated by consistent performances in 6 repeated runs. In the presence of Pt co-catalyst, the evolution rate of H_2 over PCNs is 26 times higher than that over the bulk C_3N_4 under the same conditions. The superior photocatalytic performances of PCNs can be attributed to the high surface area, good dispersity in aqueous solution, and favourable interaction with the co-catalyst nanoparticles toward efficient charge transfer.

Acknowledgements

This work was supported by National Environment Agency, Singapore under the Environment Technology Research Programme (ETRP) through Project no.: ETRP 1002 103, and SinBeRISE CREATE Programme from National Research Foundation.

Notes and references

1. X. D. Zhang and Y. Xie, *Chem. Soc. Rev.*, 2013, **42**, 8187-8199.
2. J. N. Coleman, M. Lotya, A. O'Neill, S. D. Bergin, P. J. King, U. Khan, K. Young, A. Gaucher, S. De and R. J. Smith, *Science*, 2011, **331**, 568-571.
3. V. Nicolosi, M. Chhowalla, M. G. Kanatzidis, M. S. Strano and J. N. Coleman, *Science*, 2013, **340**.
4. C. C. Han, L. Ge, C. F. Chen, Y. J. Li, X. L. Xiao, Y. N. Zhang and L. L. Guo, *Appl. Catal. B: Environ.*, 2014, **147**, 546-553.
5. M. Chhowalla, H. S. Shin, G. Eda, L.-J. Li, K. P. Loh and H. Zhang, *Nat. Chem.*, 2013, **5**, 263-275.
6. A. K. Geim and K. S. Novoselov, *Nat. Mater.*, 2007, **6**, 183-191.
7. A. Splendiani, L. Sun, Y. B. Zhang, T. S. Li, J. H. Kim, C.-Y. Chim, G. L. Galli and F. Wang, *Nano Lett.*, 2010, **10**, 1271-1275.
8. D. Voiry, H. Yamaguchi, J. Li, R. Silva, D. C. Alves, T. Fujita, M. Chen, T. Asefa, V. B. Shenoy and G. Eda, *Nat. Mater.*, 2013, **12**, 850-855.
9. D. N. Bunck and W. R. Dichtel, *J. Am. Chem. Soc.*, 2013, **135**, 14952-14955.
10. P. Niu, L. L. Zhang, G. Liu and H. M. Cheng, *Adv. Funct. Mater.*, 2012, **22**, 4763-4770.
11. S. B. Yang, Y. J. Gong, J. S. Zhang, L. Zhan, L. L. Ma, Z. Y. Fang, R. Vajtai, X. C. Wang and P. M. Ajayan, *Adv. Mat.*, 2013, **25**, 2452-2456.
12. J. Xu, L. W. Zhang, R. Shi and Y. F. Zhu, *J. Mater. Chem. A*, 2013, **1**, 14766-14772.

13. J. K. Jiang, G. Oberdörster and P. Biswas, *J. Nanopart. Res.*, 2009, **11**, 77-89.
14. X. C. Wang, K. Maeda, A. Thomas, K. Takanabe, G. Xin, J. M. Carlsson, K. Domen and M. Antonietti, *Nat. Mater.*, 2009, **8**, 76-80.
15. X. C. Wang, K. Maeda, X. F. Chen, K. Takanabe, K. Domen, Y. D. Hou, X. Z. Fu and M. Antonietti, *J. Am. Chem. Soc.*, 2009, **131**, 1680-1681.
16. G. Liu, P. Niu, C. H. Sun, S. C. Smith, Z. G. Chen, G. Q. Lu and H.-M. Cheng, *J. Am. Chem. Soc.*, 2010, **132**, 11642-11648.
17. J. D. Hong, X. Y. Xia, Y. S. Wang and R. Xu, *J. Mater. Chem.*, 2012, **22**, 15006-15012.
18. J. Ran, J. Zhang, J. Yu, M. Jaroniec and S. Z. Qiao, *Chem. Soc. Rev.*, 2014, DOI: 10.1039/C1033CS60425J.
19. M. Shalom, S. Inal, C. Fettkenhauer, D. Neher and M. Antonietti, *J. Am. Chem. Soc.*, 2013, **135**, 7118-7121.
20. K. Maeda, K. Sekizawa and O. Ishitani, *Chem. Commun.*, 2013, **49**, 10127-10129.
21. J. L. Lin, Z. M. Pan and X. C. Wang, *ACS Sustainable Chem. Eng.*, 2013, **2**, 353-358.
22. A. Kudo and Y. Miseki, *Chem. Soc. Rev.*, 2009, **38**, 253-278.
23. J. D. Hong, W. Zhang, Y. B. Wang, T. H. Zhou and R. Xu, *ChemCatChem*, 2014, **6**, 2315-2321.
24. X. D. Zhang, X. Xie, H. Wang, J. J. Zhang, B. C. Pan and Y. Xie, *J. Am. Chem. Soc.*, 2013, **135**, 18-21.
25. Y. B. Wang, J. D. Hong, W. Zhang and R. Xu, *Catal. Sci. Technol.*, 2013, **3**, 1703-1711.
26. H. Xu, J. Yan, X. J. She, L. Xu, J. X. Xia, Y. G. Xu, Y. H. Song, L. Y. Huang and H. M. Li, *Nanoscale*, 2014, **6**, 1406-1415.
27. J. Q. Tian, Q. Liu, A. M. Asiri, A. O. Al-Youbi and X. P. Sun, *Anal. Chem.*, 2013, **85**, 5595–5599.
28. J. Q. Tian, Q. Liu, C. J. Ge, Z. C. Xing, A. M. Asiri, A. O. Al-Youbic and X. P. Sun, *Nanoscale*, 2013, **5**, 8921-8924.
29. J. Q. Tian, Q. Liu, A. M. Asiri, A. H. Qusti, A. O. Al-Youbi and X. P. Sun, *Nanoscale*, 2013, **5**, 11604-11609.
30. J. Q. Tian, R. Ning, Q. Liu, A. M. Asiri, A. O. Al-Youbi and X. P. Sun, *ACS Appl. Mater. Interfaces*, 2014, **6**, 1011-1017.
31. J. Q. Tian, Q. Liu, A. M. Asiri, K. A. Alamry and X. P. Sun, *ChemSusChem*, 2014, DOI : 10.1002/cssc.201402118.
32. N. Y. Cheng, J. Q. Tian, Q. Liu, C. J. Ge, A. H. Qusti, A. M. Asiri, A. O. Al-Youbi and X. P. Sun, *ACS Appl. Mater. Interfaces*, 2013, **5**, 6815-6819.
33. L. Ge, C. C. Han, J. Liu and Y. F. Li, *Appl. Catal. A: General*, 2011, **409**, 215-222.
34. J. D. Hong, Y. S. Wang, Y. B. Wang, W. Zhang and R. Xu, *ChemSusChem*, 2013, **6**, 2263-2268.
35. Y. S. Jun, J. Park, S. U. Lee, A. Thomas, W. H. Hong and G. D. Stucky, *Angew. Chem. Int. Ed.*, 2013, **125**, 11289-11293.
36. C. P. Chen, P. Gunawan and R. Xu, *J. Mater. Chem.*, 2011, **21**, 1218-1225.
37. J. S. Zhang, M. Grzelczak, Y. D. Hou, K. Maeda, K. Domen, X. Z. Fu, M. Antonietti and X. C. Wang, *Chem. Sci.*, 2012, **3**, 443-446.
38. Y. X. Pan, H. Q. Zhuang, J. D. Hong, Z. Fang, H. Liu, B. Liu, Y. Z. Huang and R. Xu, *ChemSusChem*, 2014, **7**, 2537-2544.
39. J.-L. Capelo-Martínez, *Ultrasound in chemistry: analytical applications*, John Wiley & Sons, 2008.